

# Calculation of the biquadratic spin interactions based on the spin cluster expansion for *ab initio* tight-binding models

Tatsuto Hatanaka<sup>1,2,\*</sup>, Takuya Nomoto<sup>3,4,†</sup> and Ryotaro Arita<sup>2,4‡</sup>

<sup>1</sup> Department of Applied Physics, The University of Tokyo, Bunkyo-ku, Tokyo, 113-8656, Japan

<sup>2</sup> RIKEN Center for Emergent Matter Science (CEMS), Wako 351-0198, Japan

<sup>3</sup> Department of Physics, Tokyo Metropolitan University, Hachioji, Tokyo 192-0397, Japan

<sup>4</sup> Research Center for Advanced Science and Technology,  
The University of Tokyo, Meguro-ku, Tokyo 153-8904, Japan

(Dated: May 8, 2024)

We devise a calculation scheme for *ab initio* tight-binding Hamiltonians to evaluate the biquadratic spin interaction. This scheme employs the spin cluster expansion with the disordered local moment method and was originally developed within the Korringa-Kohn-Rostoker theory. By applying it to the two-orbital Hubbard model, we show that the evaluated biquadratic interactions agree well with those in the effective quantum spin model derived for the limit of strong correlation. This result suggests the broad applicability of the method to various magnets with large local moments. We then apply it to the *ab initio* tight-binding models for bcc Fe and fcc Ni and obtain consistent results with previous studies. The present scheme offers a convenient *ab initio* tool for understanding or predicting magnetic properties arising from the biquadratic interaction.

## I. INTRODUCTION

Recently, antiferromagnetic materials with nontrivial spin arrangements have attracted broad interest due to their unique properties, making them suitable for technological applications [1–3]. These complex spin configurations often arise from spin interactions beyond what the standard Heisenberg model accounts for. For instance, the Dzyaloshinskii-Moriya (DM) interaction [4, 5], which originates from the spin-orbit coupling, is well-known for inducing noncollinear spin structures. In addition, the biquadratic interaction, a direct extension of the bilinear Heisenberg interaction, is also essential in stabilizing such complex spin arrangements. It can play a crucial role even in the absence of the spin-orbit coupling and its effects on various spin systems have been extensively investigated from both theoretical and experimental perspectives [6–12].

Deriving realistic spin Hamiltonians for magnetic materials from first principles has been a longstanding challenge. The Liechtenstein-Katsnelson-Antropov-Gubanov (LKAG) method using the magnetic force theorem [13–15] has become a staple in the field, and has been applied across diverse materials [16–20]. With this method, we can evaluate the bilinear exchange interaction in the classical spin model by calculating how infinitesimal spin rotations affect the total energy of the quantum system under consideration. The asymptotic behavior of the exchange interaction calculated by this method is well-understood for both the strongly correlated and itinerant limits.

However, it is important to note the following two points for LKAG: The first is that the method yields only the bilinear interaction, incorporating contributions from all other higher-order terms due to its mapping process using total en-

ergy derivatives. Secondly, the method is based on a magnetically ordered reference state, which may lead to different results depending on the chosen reference state. While alternative methods have been proposed to compute higher-order or multi-spin interactions [21, 22], the issue of their dependence on a specific reference state still remains.

Another possible approach is to determine the parameters in the classical spin models by fitting the total energies of various spin configurations calculated by first-principles calculations. This method enables us to evaluate arbitrary spin interactions. However, it needs large supercells to handle complex spin structures, which can cause a problem of convergence in the calculation. It also requires a lot of computational resources, especially for large systems. Furthermore, the result of this approach depends not only on the types of interactions included in the spin Hamiltonian but also on which interactions are given priority during the fitting process.

Thus, there is a demand for methods that can evaluate higher-order or multi-spin interactions without assuming any specific magnetic order and requiring large supercells. The SCE-RDLM calculation scheme [23–28], which combines the spin cluster expansion (SCE) [29, 30] and the relativistic disordered local moment (RDLM) method [31], is one of the approaches that have such features. In the SCE framework, the energy surface of a classical spin system is systematically expanded using a complete and orthogonal basis function of spin clusters. Therefore, arbitrary interactions expressed by the basis functions are considered. Hence, we no longer need to assume a specific spin Hamiltonian in advance. Furthermore, since we consider a virtual paramagnetic state, i.e., the disordered local moment state, this approach has less dependence on the reference state than LKAG.

SCE-RDLM was originally formulated for the multiple scattering theory based on the Green’s function and implemented in the spin density functional theory (SDFT) calculations through the Korringa-Kohn-Rostoker (KKR) method. In this study, we formulate the scheme for *ab initio* tight-binding models. Our method can be widely applied to magnetic materials with large local moments and does not depend on the

\* [hatanaka-tatsuto346@g.ecc.u-tokyo.ac.jp](mailto:hatanaka-tatsuto346@g.ecc.u-tokyo.ac.jp)

† [tnomoto@tmu.ac.jp](mailto:tnomoto@tmu.ac.jp)

‡ [arita@riken.jp](mailto:arita@riken.jp)

choice of the basis of first-principles calculations. It will be a useful tool for understanding and predicting the physical properties of magnetic materials with complex spin configurations that arise from higher-order spin interactions.

The organization of the paper is as follows. In Section II, we formulate SCE-DLM, the nonrelativistic version of SCE-RDLM, for *ab initio* tight-binding models. While we can apply the approach to arbitrary spin interactions, our primary emphasis lies on the biquadratic exchange interaction which is crucial for stabilizing nontrivial spin textures in antiferromagnets, even in the absence of the relativistic spin-orbit coupling. We present computational details in Section III. We conduct benchmark calculations in Section IV to validate our approach. Specifically, we apply it to the one-dimensional two-orbital Hubbard model and two prototypical magnets, bcc Fe and fcc Ni. In the former, we analyze the asymptotic behavior of the bilinear and biquadratic interactions calculated for the limit of strong correlation and confirm that the interactions evaluated by our approach align with those evaluated for the effective quantum spin model. In the latter, we show the results for the *ab initio* tight-binding models for bcc Fe and fcc Ni. Based on these results, we discuss the difference among several previous theoretical results of the biquadratic interaction for these materials in Section V. In Section VI, we provide our conclusion.

## II. FORMULATION

### A. Spin Cluster Expansion

The spin cluster expansion (SCE) developed by Drautz and Fähnle [29, 30] provides a tool to expand systematically the energy surface of the many-body classical spin system by introducing clusters consisting of several spins. We employ a complete orthonormal basis set, namely the real spherical harmonics  $Y_{L=(l,m)}(\mathbf{e})$  for a unit vector  $\mathbf{e}$  of a classical spin, as the basis function of each spin. We then take the basis functions of clusters as a multiplication of the basis functions of each spin as follows:

$$\Phi_C^{\{L\}}(\{\mathbf{e}\}) = \frac{1}{(4\pi)^{(N-n)/2}} \prod_{i \in C} Y_{L_i}(\mathbf{e}_i) \quad (1)$$

where  $N$  refers to the number of all spins in the system,  $C$  to the cluster,  $n$  to the size of the cluster,  $\{\mathbf{e}\}$  to an array representing the spin directions, and  $\{L\}$  to an array of the degrees of freedom of the basis function of each spin in the cluster, specifically  $L = (l, m)$  for the real spherical harmonics, respectively.

We then can expand the energy surface in terms of a cluster basis. The expansion coefficients of each cluster are defined

as

$$\Omega(\{\mathbf{e}\}) = \Omega_0 + \sum_C \sum_{\{L\}} J_C^{\{L\}} \Phi_C^{\{L\}}(\{\mathbf{e}\}) \quad (2)$$

$$J_C^{\{L\}} = \langle \Phi_C^{\{L\}} | \Omega \rangle \quad (3)$$

$$\langle f | g \rangle = \int \cdots \int \left[ \prod_{i=1}^N (d^2 \mathbf{e}_i) \right] f(\{\mathbf{e}\}) g(\{\mathbf{e}\}) \quad (4)$$

where  $\Omega_0$  and  $\int d^2 \mathbf{e}$  stand for an inessential constant offset independent of the spin configuration and integration over the surface of a unit sphere, respectively. In Eq. (3), we use the useful Dirac bra-ket notation, and the inner product in this notation is defined in Eq. (4).

Hereafter, we consider the energy surface expanded up to the two-spin clusters. Note that we can perform the expansion for clusters consisting of more than two spins in a similar way.

$$\begin{aligned} \Omega(\{\mathbf{e}\}) = & \Omega_0 + \sum_i \sum_{L \neq (0,0)} J_i^L Y_L(\mathbf{e}_i) \\ & + \frac{1}{2} \sum_{i \neq j} \sum_{L, L' \neq (0,0)} J_{ij}^{LL'} Y_L(\mathbf{e}_i) Y_{L'}(\mathbf{e}_j) \end{aligned} \quad (5)$$

Each expanding coefficient for one/two spin clusters can be evaluated using the inner product in Eqs. (3) and (4).

$$J_i^L = \int d^2 \mathbf{e}_i \langle \Omega \rangle_{\mathbf{e}_i} Y_L(\mathbf{e}_i) \quad (6)$$

$$J_{ij}^{LL'} = \iint d^2 \mathbf{e}_i d^2 \mathbf{e}_j \langle \Omega \rangle_{\mathbf{e}_i, \mathbf{e}_j} Y_L(\mathbf{e}_i) Y_{L'}(\mathbf{e}_j) \quad (7)$$

$$\langle \Omega \rangle_C = \frac{1}{(4\pi)^{N-n}} \int \cdots \int \left[ \prod_{i \notin C} (d^2 \mathbf{e}_i) \right] \Omega(\{\mathbf{e}\}) \quad (8)$$

where  $\langle \Omega \rangle_C$  stands for the expectation value calculated by integrating all solid angles except for spins in the cluster  $C$ . Since we can not straightforwardly calculate Eq. (8) for many-body systems, we use the disordered local moment state which is discussed in Sec. II B.

### B. Disordered Local Moment

The coherent potential approximation (CPA) was introduced to handle the electronic structure of systems with random potentials, such as those found in alloys with random atomic species. Within the CPA, this randomness is addressed through the single-site approximation, which divides the overall potential into contributions from each on-site potential. Similarly, the disordered local moment (DLM) approach deals with randomness, where it focuses on the orientation of magnetic spins. It models a virtual paramagnetic state with randomly oriented spins, providing a way to consider a magnetically disordered state. While it was originally developed for the Korringa-Kohn-Rostoker (KKR) method, it can be formulated for the tight-binding Hamiltonian [32].

We consider the tight-binding Hamiltonian defined as

$$\mathcal{H} = \sum_{i\ell\sigma, jm\sigma'} \left( H_{i\ell\sigma, jm\sigma'} \hat{c}_{i\ell\sigma}^\dagger \hat{c}_{jm\sigma'} + \text{h.c.} \right), \quad (9)$$

where  $(i, j)$ ,  $(\ell, m)$ , and  $(\sigma, \sigma')$  are the indices of sites, orbitals, and spins, respectively. The operator  $\hat{c}_{i\ell\sigma}/\hat{c}_{i\ell\sigma}^\dagger$  stands for the annihilation/creation operator of an electron specified with the degrees of freedom  $(i\ell\sigma)$ . We divide each component of the Hamiltonian into the spin-independent off-site hopping  $t$  and the on-site magnetic potential term  $v$ ,

$$H_{i\ell\sigma, jm\sigma'} = t_{i\ell, jm} \delta_{\sigma, \sigma'} + \delta_{ij} v_{\ell, m}^i [\mathbf{e}_i \cdot \boldsymbol{\sigma}]_{\sigma\sigma'}, \quad (10)$$

where  $\mathbf{e}_i, \boldsymbol{\sigma}$  is the direction of a spin at the site  $i$  and the Pauli matrix, respectively. Here, we assume that there are no spin-dependent hopping terms and that the spin-dependent potentials  $v$ 's are a local quantity. Although there could be non-local spin-dependent potentials in the tight-binding Hamiltonian constructed from first principles, we ignore them to reduce the computational cost. We denote the former term of Eq. (10) as  $H_0$  and the latter as  $V$  such that  $H = H_0 + V$ .

In the DLM method, we consider the virtual state with randomly oriented spins and introduce the self-energy  $\Sigma$ , instead of the spin-dependent potential  $V$ , corresponding to the effective potential of such a disordered state as follows:

$$H_c = H_0 + \Sigma \quad (11)$$

$$H = H_c + (V - \Sigma), \quad (12)$$

where  $H_c$  indicates the Hamiltonian of the DLM state. Note that the introduced self-energy  $\Sigma$  is a local and spin-independent quantity so that  $\Sigma_{i\ell\sigma, jm\sigma'} = \delta_{ij} \tilde{\Sigma}_{\ell\sigma, m\sigma'}^i$ . The Green's functions in the real space are given as follows:

$$\bar{G}(z) = [z - H_c]^{-1} \quad (13)$$

$$\begin{aligned} G(z) &= [z - H]^{-1} \\ &= \bar{G}[1 + \bar{G}(V - \Sigma)]^{-1}, \end{aligned} \quad (14)$$

We also introduce the scattering matrix  $T$  as follows:

$$T_i(\mathbf{e}_i) = \left( V_i(\mathbf{e}_i) - \tilde{\Sigma}^i \right) \left[ 1 - \bar{G}_{ii} \left[ V_i(\mathbf{e}_i) - \tilde{\Sigma}^i \right] \right]^{-1} \quad (15)$$

where  $V_i(\mathbf{e}_i)$  stands for the magnetic potential of the spin at site  $i$  with the orientation  $\mathbf{e}_i$ , namely  $[V_i(\mathbf{e}_i)]_{\ell\sigma, m\sigma'} = v_{\ell, m}^i [\mathbf{e}_i \cdot \boldsymbol{\sigma}]_{\sigma\sigma'}$ , and the scattering matrix  $T_i(\mathbf{e}_i)$  has the same degrees of freedom with those of  $V_i(\mathbf{e}_i)$ . We then can formulate the CPA condition for the tight-binding Hamiltonian with the single-site approximation [32],

$$\frac{1}{4\pi} \int d^2\mathbf{e}_i T_i(\mathbf{e}_i) = 0. \quad (16)$$

In the cases without the relativistic spin-orbit coupling (SOC), the CPA condition in Eq.(16) is expressed as follows:

$$\frac{T_i(\hat{\mathbf{z}}) + T_i(-\hat{\mathbf{z}})}{2} = 0, \quad (17)$$

where  $\hat{\mathbf{z}}$  is a unit vector along the  $z$ -axis.

In the numerical calculation, we determine the self-energy and the chemical potential in a self-consistent manner [32]. We have to set the chemical potential  $\mu_c$  of the DLM state by the conservation condition for the number of electrons below,

$$N = -\frac{1}{\pi} \int d\epsilon f(\epsilon) \text{Im Tr } \bar{G}(\epsilon) \quad (18)$$

$$f(\epsilon) = \frac{1}{1 + e^{\beta(\epsilon - \mu_c)}} \quad (19)$$

where Tr stands for taking a trace about all indices of the sites, orbitals, and spins, and  $f(\epsilon)$  is the Fermi distribution function.

### C. SCE-DLM scheme

By using Lloyd's formula [33, 34] for the reference state, i.e., the DLM state, we obtain the expression for  $\langle \Omega \rangle_{\mathbf{e}_i \mathbf{e}_j}$  [23],

$$\begin{aligned} \langle \Omega \rangle_{\mathbf{e}_i \mathbf{e}_j} &= \Omega_0 - \frac{1}{\pi} \text{Im} \int^{\epsilon_F} d\epsilon \left[ \ln \det [1 + T_i(\mathbf{e}_i) \bar{G}_{ii}] \right. \\ &\quad + \ln \det [1 + T_j(\mathbf{e}_j) \bar{G}_{jj}] \\ &\quad + \sum_{l \neq i, j} \int d^2\mathbf{e}_l \ln \det [1 + T_l(\mathbf{e}_l) \bar{G}_{ll}] \\ &\quad \left. + \sum_{k=1}^{\infty} \text{Tr} \left[ (T_i(\mathbf{e}_i) \bar{G}_{ij} T_j(\mathbf{e}_j) \bar{G}_{ji})^k \right] \right] \end{aligned} \quad (20)$$

where  $\Omega_0$  stands for the energy of the DLM state. By following Eq. (7), the integration with the spherical harmonics yields the expansion coefficients for the two-spin clusters [23],

$$\begin{aligned} J_{ij}^{LL'} &= -\frac{1}{\pi} \text{Im} \int d\epsilon f(\epsilon) \iint d^2\mathbf{e}_i d^2\mathbf{e}_j Y_L(\mathbf{e}_i) Y_{L'}(\mathbf{e}_j) \\ &\quad \times \ln \det [1 - T_i(\mathbf{e}_i) \bar{G}_{ij} T_j(\mathbf{e}_j) \bar{G}_{ji}]. \end{aligned} \quad (21)$$

To map the energy expanded with the one/two-spin clusters in Eq. (2) to the following classical spin Hamiltonian,

$$\mathcal{H} = -2 \sum_{\langle i, j \rangle} [J_{ij}(\mathbf{e}_i \cdot \mathbf{e}_j) + B_{ij}(\mathbf{e}_i \cdot \mathbf{e}_j)^2], \quad (22)$$

we use the sum rule for the spherical harmonics below,

$$\frac{4\pi}{2l+1} \sum_m Y_l^m(\mathbf{e}_i) Y_l^m(\mathbf{e}_j) = P_l(\mathbf{e}_i \cdot \mathbf{e}_j) \quad (23)$$

where  $P_l(x)$  is the Legendre polynomial. Here, we consider a SOC-free case, so that the Hamiltonian has the SU(2) symmetry. Hence, the expansion coefficients  $J_{ij}^{LL'}$  do not depend on  $m$ , i.e., the spin interactions are isotropic. Given that the bilinear and biquadratic interactions in the Hamiltonian in Eq. (22) correspond to  $l = 1$  and 2, respectively, we can obtain these

parameters from the expansion coefficients  $J_{ij}^{LL'}$  as follows:

$$J_{ij} = \frac{1}{8\pi} \sum_{m=-1}^1 J_{ij}^{(1,m)(1,m)} = \frac{3}{8\pi} J_{ij}^{(1,0)(1,0)} \quad (24)$$

$$B_{ij} = \frac{3}{16\pi} \sum_{m=-2}^2 J_{ij}^{(2,m)(2,m)} = \frac{15}{16\pi} J_{ij}^{(2,0)(2,0)} \quad (25)$$

### III. COMPUTATIONAL DETAILS

#### A. SCE-DLM scheme

In the calculation, the inverse temperature  $\beta$  was set to 500 eV<sup>-1</sup>. To evaluate the Green's function in the reciprocal space, we use 256×1×1 and 24×24×24  $k$ -point grid for the one-dimensional Hubbard model and 3d transition metals, respectively. We employ the efficient Lebedev quadrature scheme [35] in the integration over solid angles.

Integrations of real energy in Eqs. (18) and (21) can be transformed to the summation over the fermionic Matsubara poles by analytical continuation. We use the intermediate representation of the Green's function [36, 37] to reduce the computational cost.

#### B. Construction of Wannier-based tight-binding model

We performed SDFT calculations for the 3d metals with the QUANTUM ESPRESSO package [38, 39] with non-relativistic pseudopotentials in PSLibrary [40]. We used the projector augmented wave method [41, 42] and the Perdew-Burke-Ernzerhof exchange-correlation functional [43].

The energy cut-off for the plane-wave basis was set to 50 Ry, and a 16×16×16  $k$ -point grid was used. We set the lattice constant as the experimental value of  $a = 2.866 \text{ \AA}$  for bcc Fe and  $a = 3.524 \text{ \AA}$  for fcc Ni.

The Wannier functions were constructed using the Wannier90 code [44–47]. The inner window to reproduce the low energy band dispersion of the DFT calculations was set from  $E_F - 10$  to  $E_F + 10$  eV, with  $E_F$  being the Fermi energy. We constructed a nine-orbital model containing one 4s, five 3d, and three 4p atomic orbitals per atom. In constructing the Wannier functions, 8×8×8 sampling  $k$ -point grid was used.

While the present calculation employs the plane-wave basis, it should be noted that the construction of the tight-binding model does not depend on the choice of the basis functions of the SDFT calculation.

## IV. RESULTS

#### A. Two-Orbital Hubbard model

We first study the one-dimensional two-orbital Hubbard model with the nearest-neighbor hopping and intra-orbital Coulomb repulsion  $U$  considered in Ref. [48]. This model

offers one of the simplest cases that exhibit the biquadratic interaction when deriving an effective quantum spin model. The Hamiltonian is defined as

$$\mathcal{H} = - \sum_{\langle i\ell, jm \rangle, \sigma} (t_{i\ell, jm} \hat{c}_{i\ell\sigma}^\dagger \hat{c}_{jm\sigma} + \text{h.c.}) + \sum_i U \hat{n}_{i\uparrow} \hat{n}_{i\downarrow} \quad (26)$$

where  $(i, j)$ ,  $(\ell, m)$  and  $\sigma$  are the degrees of freedom of sites, orbitals, and spin, respectively. The bracket  $\langle \rangle$  stands for the summation of the combinations between nearest-neighbor sites.  $\hat{c}_{i\ell\sigma}/\hat{c}_{i\ell\sigma}^\dagger$  and  $\hat{n}_{i\sigma}$  are the annihilation/creation and number operator of an electron. We show the schematic picture of the model in Fig. 1.

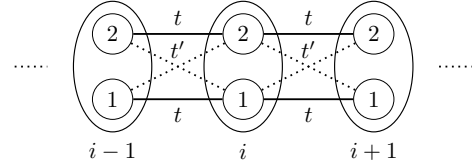


FIG. 1. One-dimensional two-orbital Hubbard model with the nearest neighbor hopping. The Hamiltonian has two types of transfer integrals,  $t$  and  $t'$ , defined for the pairs of orbitals shown with the solid and dashed lines, respectively.

While this Hamiltonian is defined using the spin-1/2 degree of freedom for each orbital, in the limit of strong correlation, we can derive an effective quantum spin model using the spin-1 degree of freedom for each site [48]:

$$\mathcal{H}_{\text{eff}} = -2 \left[ \sum_{\langle i, j \rangle} J_{ij}^{\text{Q}} (\hat{\mathbf{S}}_i \cdot \hat{\mathbf{S}}_j) + \sum_{\langle i, j \rangle} B_{ij}^{\text{Q}} (\hat{\mathbf{S}}_i \cdot \hat{\mathbf{S}}_j)^2 \right], \quad (27)$$

where the superscript Q denotes the interactions in the quantum spin model. The bilinear and biquadratic interactions can be obtained perturbatively as follows[48]:

$$J_{ij}^{\text{Q}} = -\frac{t^2 + t'^2}{U}, \quad B_{ij}^{\text{Q}} = -\frac{20t^2 t'^2}{U^3}. \quad (28)$$

Next, to compare the interactions in the quantum spin model with those in the classical spin model evaluated from SCE-DLM, denoted as  $J_{ij}^{\text{C}}$  and  $B_{ij}^{\text{C}}$ , respectively, we take the classical limit of the quantum spin [49]. For a  $S$ -spin case, the interactions need to be rescaled as follows [50]:

$$J_{ij}^{\text{Q}} (\hat{\mathbf{S}}_i \cdot \hat{\mathbf{S}}_j) \rightarrow S^2 J_{ij}^{\text{C}} (\mathbf{e}_i \cdot \mathbf{e}_j) \quad (29)$$

$$B_{ij}^{\text{Q}} (\hat{\mathbf{S}}_i \cdot \hat{\mathbf{S}}_j)^2 \rightarrow S^4 B_{ij}^{\text{C}} (\mathbf{e}_i \cdot \mathbf{e}_j)^2. \quad (30)$$

Hence, we compare  $J_{ij}^{\text{C}}$  with  $J_{ij}^{\text{Q}}$ , and likewise,  $B_{ij}^{\text{C}}$  with  $B_{ij}^{\text{Q}}$ , given that we are currently examining the spin-1 case, where  $S = 1$ .

To apply SCE-DLM to this model, we first construct a tight-binding Hamiltonian including both the hopping parameter  $t$  and spin splitting  $B$ , which can be obtained via the mean-field approximation for the half-filled state of the Hamiltonian

Eq. (26):

$$\mathcal{H}_{\text{MF}} = - \sum_{\langle il,jm \rangle, \sigma} (t_{il,jm} \hat{c}_{i\ell\sigma}^\dagger \hat{c}_{jm\sigma} + \text{h.c.}) - \mathbf{B}_i \cdot \hat{\mathbf{m}}_i \quad (31)$$

$$\mathbf{B}_i = \frac{U}{2} \langle \hat{\mathbf{m}}_i \rangle, \quad \hat{\mathbf{m}}_i = \sum_{\ell, \sigma, \sigma'} \hat{c}_{i\ell\sigma}^\dagger \boldsymbol{\sigma} \hat{c}_{i\ell\sigma'} \quad (32)$$

For the half-filled case with  $t \ll U$ , the magnetization operator  $\hat{\mathbf{m}}_i$  becomes  $\sigma_z \hat{z}$ . Consequently, we can obtain the Hubbard parameter  $U$  from the magnitude of the spin splitting  $B = |\mathbf{B}|$ , i.e.,  $U = 2B$ .

In Fig. 2, we plot  $J_{ij}^C, J_{ij}^Q, B_{ij}^C, B_{ij}^Q$  for the half-filled case as a function of  $t/U$ . It is worth noting that the chemical potential  $\mu_c$  of the DLM state is always zero for the half-filled state. We can see that the interactions evaluated perturbatively for the quantum spin model align closely with those derived from SCE-DLM in the limit of  $t/U \rightarrow 0$ . This result suggests that the present method is applicable to a wide variety of strongly correlated magnetic compounds.

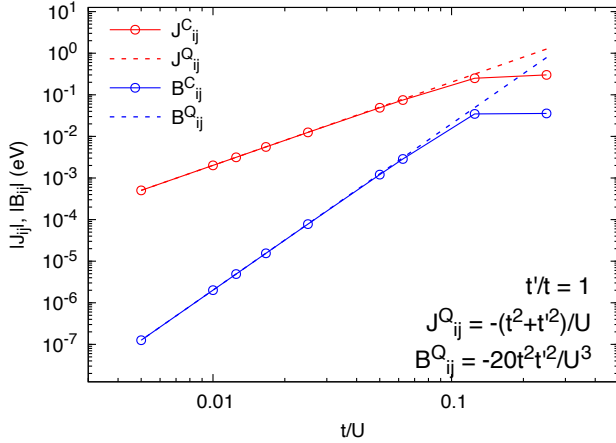


FIG. 2. Bilinear ( $J_{ij}^C/J_{ij}^Q$ ) and biquadratic ( $B_{ij}^C/B_{ij}^Q$ ) interactions in the classical/quantum spin Hamiltonian for  $t = t'$  in the limit of strong correlation  $t \ll U$ .  $J_{ij}^C$  (solid red line) and  $B_{ij}^C$  (solid blue line) are evaluated by SCE-DLM, and  $J_{ij}^Q$  (dashed red line) and  $B_{ij}^Q$  (dashed blue line) are evaluated perturbatively (see Eq. (28)).

### B. 3d transition metals

We then applied our scheme to the *ab initio* tight-binding models for the prototypical magnetic metals, bcc Fe and fcc Ni. In Fig. 3, we present the band structures of bcc Fe and fcc Ni obtained by SDFT calculations and those fitted by the Wannier-based tight-binding model.

In Fig. 4, we show the density of states (DOS) and integrated DOS along with the calibrated chemical potential  $\mu_c$  for the DLM state. Let us now compare the chemical potential ( $\mu$ ) and magnetic moment of the DLM and ferromagnetic (FM) state. Following the procedure outlined in

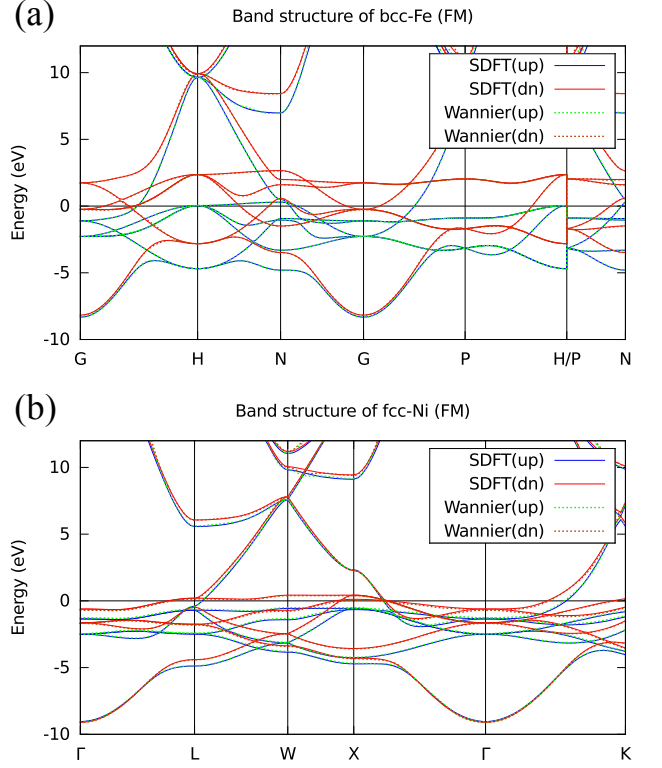


FIG. 3. Band structure of (a) bcc Fe and (b) fcc Ni. Blue and red lines are those for the up and down spin components obtained by SDFT calculation, and green and orange lines are those obtained by Wannier interpolation.

Refs. [32, 51], we calculated the DOS for each spin component of the DLM state by calculating the Green's function:

$$\overline{G}_{ii}^{\sigma\sigma} = \overline{G}_{ii} + \overline{G}_{ii} T_i(\sigma \hat{z}) \overline{G}_{ii}. \quad (33)$$

$\mu_c$ , the chemical potential of the DLM state measured from that of the FM state, is 0.55 eV for bcc Fe and -0.15 eV for fcc Ni. Namely,  $\mu$  of bcc Fe depends more sensitively on the changes in the electronic/magnetic structure compared to fcc Ni. Regarding the magnetic moment, which is defined as the difference in the number of the spin-up and spin-down electrons up to the chemical potential, for bcc Fe, it is 2.27 (2.28)  $\mu_B$  for the FM (DLM) state. For fcc Ni, it is 0.66 (0.48)  $\mu_B$  for the FM (DLM) state.

We then evaluate the nearest-neighbor (NN) bilinear ( $J$ ) and biquadratic ( $B$ ) interactions by SCE-DLM. In Fig. 5, we plot  $J$  and  $B$  as a function of  $\mu$ . For  $J$ , we compare the result with that obtained by LKAG. We see that these methods give a similar  $\mu$  dependence. It should be noted that this  $\mu$  dependence qualitatively explains the magnetism observed in 3d transition metals [16]. Another point to note in the calculation of  $J$  and  $B$  is that we should take the values at  $\mu = \mu_c$  ( $\mu = 0$ ) in the SCE-DLM (LKAG) method. Since  $\mu_c$  for Fe is quite large (0.55eV),  $J$  calculated by SCE-DLM is quite different from (much larger than) that obtained by LKAG. For Ni, these methods give similar  $J$ . Regarding  $B$ , we see that its energy scale is much smaller than that of  $J$ . While  $B$  shows

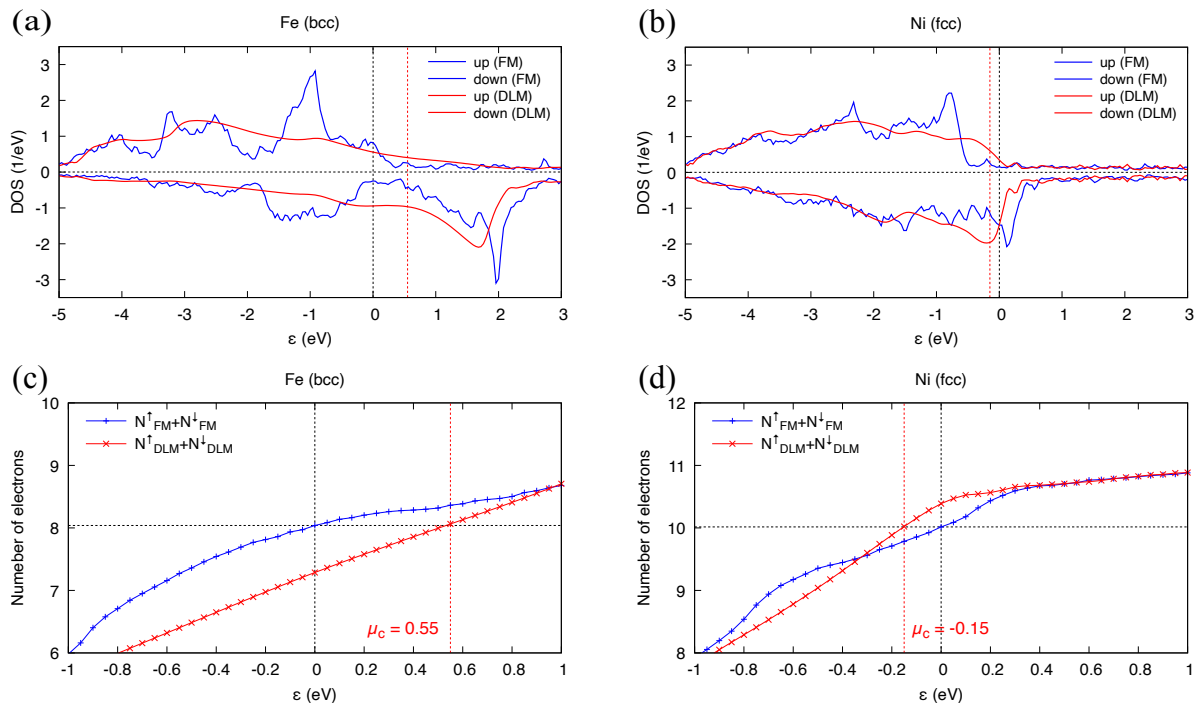


FIG. 4. Density of states (DOS) for the spin-up and spin-down components (panels (a) and (b)) and the integrated DOS (panels (c) and (d)). Panels (a) and (c) are the results for bcc Fe, while panels (b) and (d) are those for fcc Ni. In panels (a) and (b), blue lines represent the DOS for the ferromagnetic (FM) state, and red lines for the disordered local moment (DLM) state. The spin-up and spin-down components of both the FM and DLM states are plotted on the positive and negative sides, respectively. In panels (c) and (d), the vertical black lines indicate the chemical potential of the FM state ( $\mu = 0$ ), and the vertical red lines indicate the chemical potential  $\mu_c$  for the DLM state. The horizontal line indicates the number of electrons at  $\mu = 0$  in the *ab initio* tight-binding Hamiltonian.

many sign changes as a function of  $\mu$ ,  $B$  is negative at  $\mu = \mu_c$  for both bcc Fe and fcc Ni.

In Fig. 6, we plot the bilinear ( $J_{ij}$ ) and biquadratic ( $B_{ij}$ ) interactions as a function of the distance ( $R$ ) between the  $i$ -th and  $j$ -th site for the range of  $-0.1 \leq \mu \leq 0.1$  (LKAG) and  $\mu_c - 0.1 \leq \mu \leq \mu_c + 0.1$  (SCE-DLM). From Fig. 6(a), (b), (d) and (e), we see that the  $\mu$  dependence around  $\mu = 0$  ( $\mu_c$ ) of the NN interaction  $J$  is significant for bcc Fe (fcc Ni) in the LKAG (SCE-DLM) calculation, which could cause sizable computational errors in the evaluation of  $J$ . In addition, what we observe from Fig. 6 are: (a) For bcc Fe, the second NN  $J_{ij}$  calculated by LKAG is as large as the NN interaction  $J$ , which aligns with the previous study based on the KKR method [52]. (c) For bcc Fe, the size of the second NN  $B_{ij}$  is as large as that of the NN interaction  $B$ , which also aligns with the results of the fitting approach [52]. The  $\mu$  dependence of the NN interaction  $B$  (the second NN  $B_{ij}$ ) is insignificant (significant). (d) For fcc Ni, while the NN interaction  $B$  has a considerable  $\mu$  dependence, the distant interactions  $B_{ij}$  are all negligibly small.

## V. DISCUSSION

Since it is difficult to determine the biquadratic interaction directly from experiments, a variety of methods to calculate

the biquadratic interaction from first principles have been proposed. So far, theoretical calculations for bcc Fe have yielded both positive[22, 53] and negative values[21, 52, 54–56] for the biquadratic interaction. Though all results for fcc Ni consistently show negative values[21, 22], there are fewer studies compared to bcc Fe.

Except for Refs. [52, 53], these works are based on LKAG and rely on the ferromagnetic reference state to evaluate the biquadratic interaction. Our SCE-DLM approach differs from such approaches in that we need no ordered reference state. As is outlined in Ref. [57], approaches with a magnetically ordered state are valid for calculating physical properties related to the specific ordered state, such as the magnon spectrum [21]. In contrast, approaches without an ordered state are better suited for exploring properties of states far from such ordered states, e.g., constructing a phase diagram of the system.

While both of Refs. [52, 53] are based on the fitting approach, the details of these methods are different from each other. In Ref. [52], they fit the spin Hamiltonian to the *ab initio* energies for a number of spin spiral states with random wave vectors. Though they confine the spin Hamiltonian up to the biquadratic interaction and a four-spin interaction, they do not prioritize interactions between specific pairs during the fitting. On the other hand, in Ref. [53], while considering arbitrary spin interactions in the spin cluster expansion, they

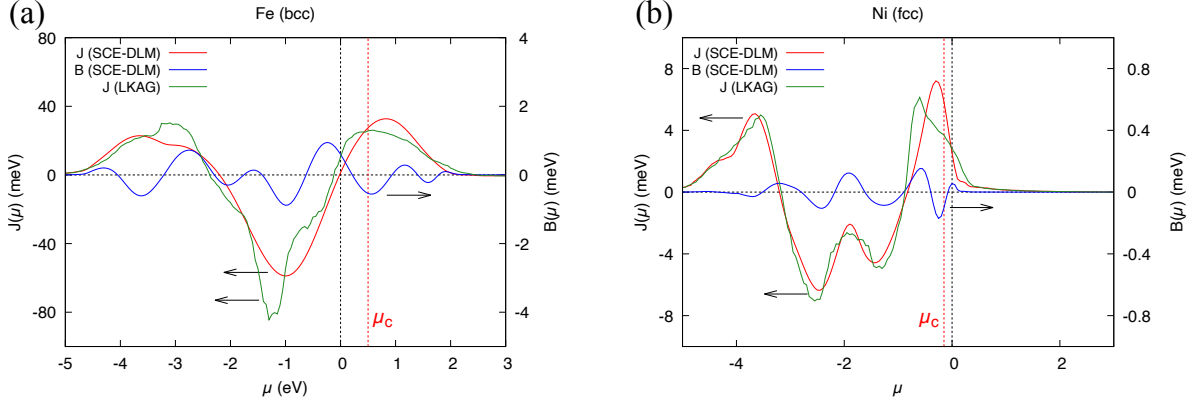


FIG. 5. Chemical potential dependence of the bilinear ( $J$ ) and biquadratic ( $B$ ) interactions for bcc Fe (a) and fcc Ni (b). Red, blue, and green lines indicate  $J$  and  $B$  calculated by SCE-DLM and  $J$  calculated by LKAG, respectively. The vertical red lines stand for the chemical potential for the DLM state  $\mu_c$ . Refer to the left vertical axis for  $J$ , and to the right vertical axis for  $B$ .

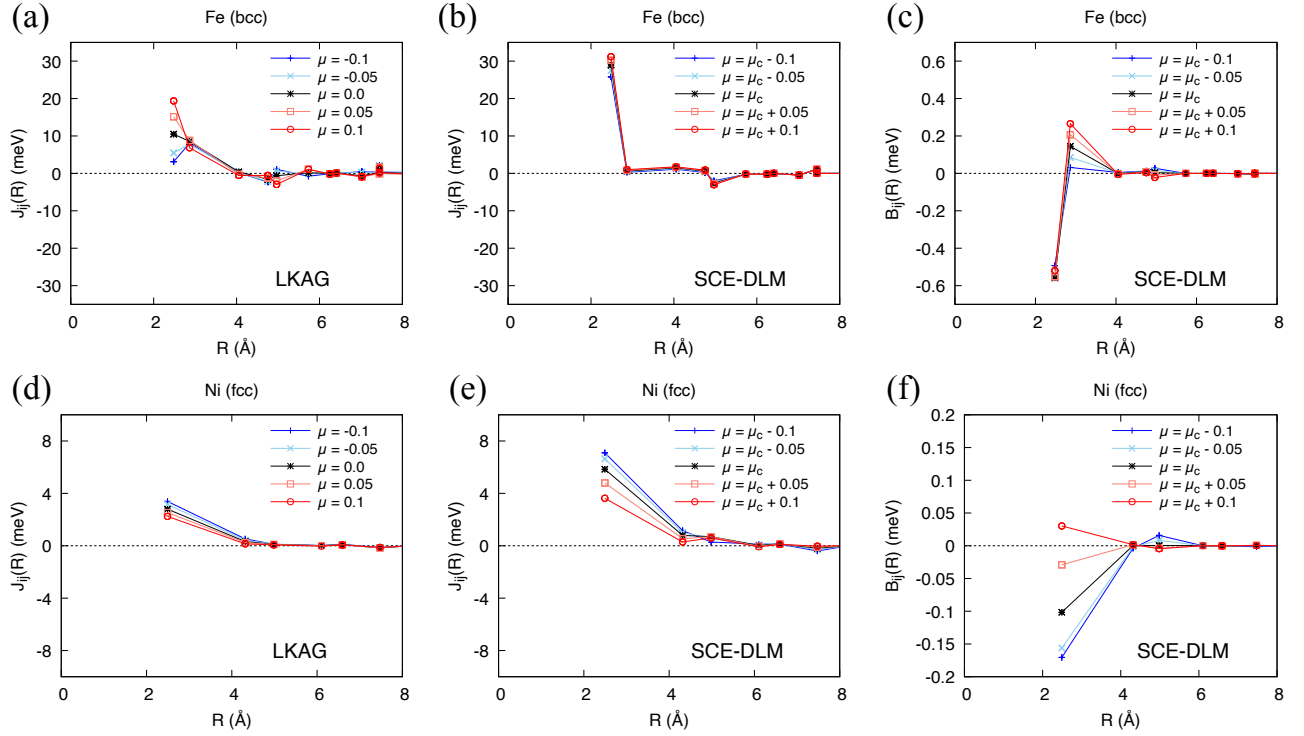


FIG. 6. The distance dependence of the bilinear ( $J_{ij}$ ) and the biquadratic ( $B_{ij}$ ) interactions. Panels (a)-(c) are the results for bcc Fe, and (d)-(f) are for fcc Ni.  $J_{ij}$  calculated by LKAG are shown in panels (a) and (d).  $J_{ij}$  ( $B_{ij}$ ) calculated by SCE-DLM are shown in panels (b) and (e) ((c) and (f)). We also plot the values when we change  $\mu$ .

estimate the nearest-neighbor biquadratic interaction after the nearest-neighbor bilinear interaction. These differences lead to the difference in the sign of the calculated biquadratic interactions.

On top of that, as illustrated in Figs. 6 (a)-(f), the chemical potential dependence of the spin interactions could introduce ambiguity in theoretical results. Our approach is similar to the approach employed in Ref. [52] regarding the accessibility to various spin configurations, and our results are consistent with their result.

## VI. CONCLUSION

We developed SCE-DLM for the tight-binding Hamiltonian by combining the spin cluster expansion and the disordered local moment method. We first applied the scheme to the two-orbital Hubbard model and examined its validity. We found that the calculated biquadratic interactions closely align with those for the effective quantum spin model. This alignment suggests the broad applicability of the scheme to a wide va-

riety of strongly correlated compounds with large local magnetic moments. We subsequently applied this scheme to two prototypical magnets, bcc Fe and fcc Ni. Our results are consistent with previous research, affirming the reliability of the method. Our approach has the advantage of not requiring a reference state and being independent of the the basis functions of first-principles calculations. It will be a convenient tool for understanding or predicting nontrivial magnetic properties induced by higher order spin interactions.

## ACKNOWLEDGEMENTS

We would like to thank Katsuhiko Tanaka, Hiroshi Katsumoto, and Juba Bouaziz for fruitful discussions. This work was supported by RIKEN Junior Research Associate Program. We acknowledge the financial support by Grant-in-Aids for Scientific Research (JSPS KAKENHI) Grant Numbers JP21H04437, JP21H04990, JP19H05825, JP22H00290, and JP24K00581, JST-CREST No. JPMJCR18T3, No. JPMJCR23O4, JST-ASPIRE No. JPMJAP2317, JST-Mirai No. JPMJMI20A1. T. N. was supported by JST, PRESTO Grant Number JPMJPR20L7, Japan.

### Appendix A: Asymptotic form for single-orbital tight-binding model

In Section IV A, a tight-binding Hamiltonian with a spin splitting was derived from the two-orbital Hubbard Hamiltonian. Here, let us look into a simpler case, i.e., a one-dimensional single-orbital model with the mean-field approximation:

$$\mathcal{H} = - \sum_{\langle i,j \rangle, \sigma} (t c_{i\sigma}^\dagger c_{j\sigma} + \text{h.c.}) - B\sigma_z. \quad (\text{A1})$$

We can analytically obtain the on-site component of the Green's function of the DLM state for this model as follows:

$$\bar{G}_{ii}(\epsilon) = \left\{ \text{sgn}(\text{Re}(\epsilon - \tilde{\Sigma}^i)) \sqrt{(\epsilon - \tilde{\Sigma}^i)^2 - 4t^2} \right\}^{-1}. \quad (\text{A2})$$

By substituting this expression of  $\bar{G}_{ii}$  to Eqs. (15) and (16) with  $V(\pm\hat{z}) = \mp B$  for the up and down spins, the CPA condition yields the equation for the self-energy  $\Sigma$  as follows:

$$0 = 2\epsilon\tilde{\Sigma}^3 - (2B^2 - 4t^2 + \epsilon^2)\tilde{\Sigma}^2 + B^4 \quad (\text{A3})$$

Let us now consider deriving the asymptotic expression of the exchange interaction for the limit of strong and weak correlation based on SCE-DLM. Starting with Eq. (21), we expand it as follows:

$$\begin{aligned} J_{ij}^{LL'} &\sim \frac{1}{\pi} \text{Im} \int d\epsilon f(\epsilon) \iint d^2\mathbf{e}_i d^2\mathbf{e}_j Y_L(\mathbf{e}_i) Y_{L'}(\mathbf{e}_j) \\ &\times \left[ T_i(\mathbf{e}_i) \bar{G}_{ij} T_j(\mathbf{e}_j) \bar{G}_{ji} + \right. \\ &\left. \frac{1}{2} T_i(\mathbf{e}_i) \bar{G}_{ij} T_j(\mathbf{e}_j) \bar{G}_{ji} T_i(\mathbf{e}_i) \bar{G}_{ij} T_j(\mathbf{e}_j) \bar{G}_{ji} \right], \end{aligned} \quad (\text{A4})$$

Here, we utilize the Taylor expansion,  $\log(1-x) \sim -x - x^2/2$ . Though there are other higher-order terms in the expansion, these terms are sufficient to obtain leading-order terms of the bilinear and biquadratic interactions in the strong and itinerant limits. We also derive the expression of the scattering operator  $T_i(\mathbf{e}_i)$  by applying the CPA condition in Eq.(A3) and introducing the inverse of the Green's function as  $A = 1/\bar{G}_{ii}(\epsilon)$ ,

$$T_i(\mathbf{e}_i) = - \frac{BA^2}{(A + \tilde{\Sigma})^2 - B^2} \begin{pmatrix} \cos \theta & e^{-i\phi} \sin \theta \\ e^{i\phi} \sin \theta & -\cos \theta \end{pmatrix}. \quad (\text{A5})$$

### 1. Itinerant limit

In the limit of  $B \ll t$ , the CPA condition becomes  $0 = 2\epsilon\tilde{\Sigma}^3 + (4t^2 - \epsilon^2)\tilde{\Sigma}^2$  and the solutions of this equation are:

$$\tilde{\Sigma}(\epsilon) = 0, \quad \frac{\epsilon}{2} + \frac{2t^2}{\epsilon} \quad (\text{A6})$$

As the latter solution is unphysical in the limit of  $\epsilon \rightarrow \pm\infty$ , the solution of the CPA condition approaches  $\tilde{\Sigma}(\epsilon) \rightarrow 0$ . By substituting this self-energy solution to Eq. (A5), the scattering operator becomes

$$T_i(\mathbf{e}_i) \rightarrow -B \begin{pmatrix} \cos \theta & e^{-i\phi} \sin \theta \\ e^{i\phi} \sin \theta & -\cos \theta \end{pmatrix}. \quad (\text{A7})$$

We here use that  $A \rightarrow \sqrt{\epsilon^2 - 4t^2}$ . The first term of the right-hand side in Eq. (A4) remains finite only for  $l = 1$ . This corresponds to the fact that higher-order interactions ( $l \geq 2$ ) require perturbations higher than the second order. It is also important to note again that  $J_{ij}^{(l,m)(l,m)}$  depends solely on  $l$  and is independent of  $m$  in the absence of SOC. Then, we can easily show that the bilinear interaction in SCE-DLM (Eq. (A4)) becomes equivalent to that of LKAG in this limit, hence yielding the RKKY interaction [58–60] as follows:

$$\begin{aligned} J_{ij} &= \frac{3}{8\pi} J_{ij}^{(1,0)(1,0)} \\ &\rightarrow \frac{B^2}{\pi N^2} \sum_{k,q} \text{Im} \int d\epsilon f(\epsilon) G_{k+q}^0 G_k^0 e^{iqR_{ij}} \\ &= \frac{B^2}{\pi N} \sum_q \chi(q) e^{iqR_{ij}}, \end{aligned} \quad (\text{A8})$$

where  $N, G_k^0 = (\epsilon - \epsilon_k + i\delta)^{-1}$ ,  $\chi(q)$  is the number of sites, the retarded Green's function, and the spin susceptibility of non-interacting electrons, respectively. Here we use an infinitesimally small value  $\delta$ , and  $\chi(q)$  is defined as follows:

$$\chi(q) = \frac{1}{\pi N} \sum_k \text{Im} \int d\epsilon f(\epsilon) G_{k+q}^0 G_k^0 \quad (\text{A9})$$

$$= \frac{1}{N} \sum_k \frac{f(\epsilon_k) - f(\epsilon_{k+q})}{\epsilon_{k+q} - \epsilon_k + i\delta}. \quad (\text{A10})$$

With SCE-DLM, we can obtain higher-order interactions such as the biquadratic interaction. Indeed, we can derive the

biquadratic interaction by considering higher order terms in Eq. (A4). The asymptotic expression of the biquadratic interaction becomes:

$$B_{ij} = \frac{15}{16\pi} J_{ij}^{(2,0)(2,0)} \rightarrow -\frac{B^4}{\pi N^2} \sum_{k,q} \text{Im} \int d\epsilon f(\epsilon) (G_{k+q}^0 G_k^0)^2 e^{iqR_{ij}}. \quad (\text{A11})$$

This always yields a negative biquadratic interaction between any sites and causes instability of the collinear spin structures, as discussed in Ref. [6].

## 2. Strongly correlated limit

In the limit of strong correlation  $U \sim B \gg t$ , the CPA condition becomes to  $2\epsilon\tilde{\Sigma}^3 - (2B^2 + \epsilon^2)\tilde{\Sigma}^2 + B^4 = 0$  and the solutions are given as:

$$\tilde{\Sigma}(\epsilon) = \frac{B^2}{\epsilon}, \frac{\epsilon \pm \sqrt{\epsilon^2 + 8B^2}}{4}. \quad (\text{A12})$$

Similarly to the itinerant case, the solution of the self-energy is  $\tilde{\Sigma}(\epsilon) \rightarrow B^2/\epsilon$ .

We start from the DLM state without the hopping term  $t$ . The retarded Green's function for this non-perturbed state is provided as:

$$\overline{G}_{ii}^{(0)}(\epsilon) = \frac{\delta_{ij}}{\epsilon - \Sigma + i\delta}, \quad (\text{A13})$$

where the superscript (0) stands for the non-perturbed term. By treating the hopping term as the perturbation, we can derive the expression for the Green's function, considering terms up to the first order perturbation:

$$\begin{aligned} \overline{G}_{ij}^{(1)}(\epsilon) &= \frac{1}{\epsilon - \tilde{\Sigma} + i\delta} t \frac{1}{\epsilon - \tilde{\Sigma} + i\delta} \\ &= \frac{t}{(\epsilon - \tilde{\Sigma} + i\delta)^2}, \end{aligned} \quad (\text{A14})$$

where the superscript (1) stands for the first order perturbation term and  $j$  is the nearest-neighbor sites of site  $i$ .

Subsequently, we evaluate the scattering operator as follows:

$$T_i(e_i) \rightarrow -\frac{(\epsilon - \tilde{\Sigma})^2}{\epsilon^2 - B^2} B \begin{pmatrix} \cos \theta & e^{-i\phi} \sin \theta \\ e^{i\phi} \sin \theta & -\cos \theta \end{pmatrix}, \quad (\text{A15})$$

where we use  $A \rightarrow \epsilon - \tilde{\Sigma}$  in this limit. By substituting Eqs. (A14) and (A15) into the first term of Eq. (A4), we obtain the following asymptotic expression for the  $l = 1$  interaction

between nearest neighbor sites:

$$\begin{aligned} J_{ij}^{(1,m)(1,m)} &\sim -\frac{2}{\pi} \frac{4\pi}{3} \text{Im} \int^{\epsilon_F} d\epsilon \frac{t^2 B^2}{(\epsilon - \Sigma + i\delta)^4} \frac{(\epsilon - \Sigma)^4}{(\epsilon^2 - B^2)^2} \\ &= -\frac{4}{3i} \int_C \frac{dz}{\text{Im}[z]} \frac{t^2 B^2}{(z - B)^2 (z + B)^2}. \end{aligned} \quad (\text{A16})$$

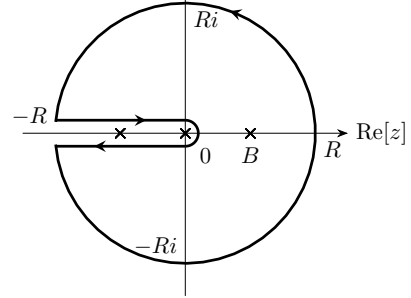


FIG. 7. Integration contour of Eq. (A16). We take the  $R \rightarrow \infty$  limit in the integration.

We illustrate an integration contour in Eq. (A16) in Fig. 7.

We subsequently derive an asymptotic expression for the bilinear interaction.

$$J_{ij} = \frac{3}{8\pi} J_{ij}^{(1,0)(1,0)} \rightarrow -\frac{t^2}{4B} \sim -\frac{t^2}{2U} \quad (\text{A17})$$

We can obtain the expression for the biquadratic interaction by following the same process.

$$B_{ij} = \frac{15}{16\pi} J_{ij}^{(2,0)(2,0)} \rightarrow -\frac{5}{4} \frac{t^4}{U^3}. \quad (\text{A18})$$

These asymptotic expressions for the bilinear and biquadratic interactions are equivalent to those obtained by the conventional LKAG method and its extensions[22] in both the strongly correlated and the itinerant limits. However, it is crucial to recognize that the initial magnetic state in SCE-DLM, the DLM state, differs from the ferromagnetic state used in these methods. Furthermore, it is noteworthy that when using SCE-DLM and the method described in Ref. [22], the biquadratic interaction remains finite even in a single-orbital system, in contrast to the effective quantum spin model where this term inevitably vanishes. In the quantum spin model of a  $S = 1/2$  system, this term corresponding to a fourth-order perturbation is merely a correction to the bilinear interaction. However, the classical treatment of spins in electron systems ensures that these higher-order interactions remain finite even in a single-orbital system. Therefore, it is not appropriate to simply compare this expression with Eq. (28).

[1] T. Jungwirth, X. Marti, P. Wadley, and J. Wunderlich, Antiferromagnetic spintronics, *Nature Nanotechnology* **11**, 231 (2016).

[2] V. Baltz, A. Manchon, M. Tsoi, T. Moriyama, T. Ono, and Y. Tserkovnyak, Antiferromagnetic spintronics, *Rev. Mod. Phys.*

- Phys. **90**, 015005 (2018).
- [3] T. Jungwirth, J. Sinova, A. Manchon, X. Marti, J. Wunderlich, and C. Felser, The multiple directions of antiferromagnetic spintronics, *Nature Physics* **14**, 200 (2018).
- [4] I. Dzyaloshinsky, A thermodynamic theory of “weak” ferromagnetism of antiferromagnetics, *Journal of Physics and Chemistry of Solids* **4**, 241 (1958).
- [5] T. Moriya, Anisotropic superexchange interaction and weak ferromagnetism, *Phys. Rev.* **120**, 91 (1960).
- [6] S. Hayami, R. Ozawa, and Y. Motome, Effective bilinear-biquadratic model for noncoplanar ordering in itinerant magnets, *Phys. Rev. B Condens. Matter* **95**, 224424 (2017).
- [7] S. Okumura, S. Hayami, Y. Kato, and Y. Motome, Magnetic hedgehog lattice in a centrosymmetric cubic metal, *Journal of the Physical Society of Japan* **91**, 093702 (2022), <https://doi.org/10.7566/JPSJ.91.093702>.
- [8] S. Seo, S. Hayami, Y. Su, S. M. Thomas, F. Ronning, E. D. Bauer, J. D. Thompson, S.-Z. Lin, and P. F. S. Rosa, Spin-texture-driven electrical transport in multi-q antiferromagnets, *Communications Physics* **4**, 58 (2021).
- [9] B. G. Ueland, C. F. Miclea, Y. Kato, O. Ayala-Valenzuela, R. D. McDonald, R. Okazaki, P. H. Tobash, M. A. Torrez, F. Ronning, R. Movshovich, Z. Fisk, E. D. Bauer, I. Martin, and J. D. Thompson, Controllable chirality-induced geometrical hall effect in a frustrated highly correlated metal, *Nature Communications* **3**, 1067 (2012).
- [10] J. A. M. Paddison, H. Zhang, J. Yan, M. J. Cliffe, S.-H. Do, S. Gao, M. B. Stone, D. Dahlbom, K. Barros, C. D. Batista, and A. D. Christianson, Cubic double perovskites host noncoplanar spin textures (2023), [arXiv:2301.11395 \[cond-mat.str-el\]](https://arxiv.org/abs/2301.11395).
- [11] H. Takagi, R. Takagi, S. Minami, T. Nomoto, K. Ohishi, M. T. Suzuki, Y. Yanagi, M. Hirayama, N. D. Khanh, K. Karube, H. Saito, D. Hashizume, R. Kiyonagi, Y. Tokura, R. Arita, T. Nakajima, and S. Seki, Spontaneous topological hall effect induced by non-coplanar antiferromagnetic order in intercalated van der waals materials, *Nature Physics* **19**, 961 (2023).
- [12] P. Park, W. Cho, C. Kim, Y. An, Y.-G. Kang, M. Avdeev, R. Sibille, K. Iida, R. Kajimoto, K. H. Lee, W. Ju, E.-J. Cho, H.-J. Noh, M. J. Han, S.-S. Zhang, C. D. Batista, and J.-G. Park, Tetrahedral triple-q magnetic ordering and large spontaneous hall conductivity in the metallic triangular antiferromagnet  $\text{Co}_1/3\text{Ta}_2\text{S}_2$ , *Nature Communications* **14**, 8346 (2023).
- [13] T. Oguchi, K. Terakura, and N. Hamada, Magnetism of iron above the curie temperature, *Journal of Physics F: Metal Physics* **13**, 145 (1983).
- [14] A. I. Liechtenstein, M. I. Katsnelson, and V. A. Gubanov, Exchange interactions and spin-wave stiffness in ferromagnetic metals, *Journal of Physics F: Metal Physics* **14**, L125 (1984).
- [15] T. Nomoto, T. Koretsune, and R. Arita, Local force method for the ab initio tight-binding model: Effect of spin-dependent hopping on exchange interactions, *Phys. Rev. B* **102**, 014444 (2020).
- [16] A. Sakuma, First principles study on the exchange constants of the 3d transition metals, *Journal of the Physical Society of Japan* **68**, 620 (1999), <https://doi.org/10.1143/JPSJ.68.620>.
- [17] A. Sakuma, First-principles study on the non-collinear magnetic structures of disordered alloys, *Journal of the Physical Society of Japan* **69**, 3072 (2000), <https://doi.org/10.1143/JPSJ.69.3072>.
- [18] Y. Nomura, T. Nomoto, M. Hirayama, and R. Arita, Magnetic exchange coupling in cuprate-analog  $d^9$  nickelates, *Phys. Rev. Res.* **2**, 043144 (2020).
- [19] T. Nomoto, T. Koretsune, and R. Arita, Formation mechanism of the helical  $q$  structure in gd-based skyrmion materials, *Phys. Rev. Lett.* **125**, 117204 (2020).
- [20] T. Hatanaka, T. Nomoto, and R. Arita, Magnetic interactions in intercalated transition metal dichalcogenides: A study based on *ab initio* model construction, *Phys. Rev. B* **107**, 184429 (2023).
- [21] A. Szilva, M. Costa, A. Bergman, L. Szunyogh, L. Nordström, and O. Eriksson, Interatomic exchange interactions for finite-temperature magnetism and nonequilibrium spin dynamics, *Phys. Rev. Lett.* **111**, 127204 (2013).
- [22] S. Mankovsky, S. Polesya, and H. Ebert, Extension of the standard heisenberg hamiltonian to multispin exchange interactions, *Phys. Rev. B* **101**, 174401 (2020).
- [23] L. Szunyogh, L. Udvardi, J. Jackson, U. Nowak, and R. Chantrell, Atomistic spin model based on a spin-cluster expansion technique: Application to the  $\text{IrMn}_3/\text{Co}$  interface, *Phys. Rev. B* **83**, 024401 (2011).
- [24] E. Simon, R. Yanes, S. Khmelevskiy, K. Palotás, L. Szunyogh, and U. Nowak, Magnetism and exchange-bias effect at the  $\text{mnn}/\text{Fe}$  interface, *Phys. Rev. B* **98**, 094415 (2018).
- [25] B. Nyári, A. Deák, and L. Szunyogh, Weak ferromagnetism in hexagonal  $\text{Mn}_3z$  alloys ( $z = \text{Sn, Ge, Ga}$ ), *Phys. Rev. B* **100**, 144412 (2019).
- [26] E. Simon, A. Donges, L. Szunyogh, and U. Nowak, Non-collinear antiferromagnetic states in ru-based heusler compounds induced by biquadratic coupling, *Phys. Rev. Mater.* **4**, 084408 (2020).
- [27] T. Dannegger, A. Deák, L. Rózsa, E. Galindez-Ruales, S. Das, E. Baek, M. Kläui, L. Szunyogh, and U. Nowak, Magnetic properties of hematite revealed by an ab initio parameterized spin model, *Phys. Rev. B* **107**, 184426 (2023).
- [28] A. Deák, L. Szunyogh, and B. Ujfalussy, Thickness-dependent magnetic structure of ultrathin  $\text{Fe}/\text{Ir}(001)$  films: From spin-spiral states toward ferromagnetic order, *Phys. Rev. B Condens. Matter* **84**, 224413 (2011).
- [29] R. Drautz and M. Fähnle, Spin-cluster expansion: Parametrization of the general adiabatic magnetic energy surface with ab initio accuracy, *Phys. Rev. B* **69**, 104404 (2004).
- [30] R. Drautz and M. Fähnle, Parametrization of the magnetic energy at the atomic level, *Phys. Rev. B* **72**, 212405 (2005).
- [31] A. J. Pindor, J. Staunton, G. M. Stocks, and H. Winter, Disordered local moment state of magnetic transition metals: a self-consistent kkr cpa calculation, *Journal of Physics F: Metal Physics* **13**, 979 (1983).
- [32] N. Ito, T. Nomoto, K. Kobayashi, S. Mankovsky, K. Nomura, R. Arita, H. Ebert, and T. Koretsune, Wannier-based implementation of the coherent potential approximation with applications to fe-based transition metal alloys, *Phys. Rev. B* **105**, 125136 (2022).
- [33] P. Lloyd, Wave propagation through an assembly of spheres: Ii. the density of single-particle eigenstates, *Proceedings of the Physical Society* **90**, 207 (1967).
- [34] R. Zeller, Lloyd’s formula in multiple-scattering calculations with finite temperature, *Journal of Physics: Condensed Matter* **17**, 5367 (2005).
- [35] V. Lebedev, Quadratures on a sphere, *USSR Computational Mathematics and Mathematical Physics* **16**, 10 (1976).
- [36] H. Shinaoka, J. Otsuki, M. Ohzeki, and K. Yoshimi, Compressing green’s function using intermediate representation between imaginary-time and real-frequency domains, *Phys. Rev. B* **96**, 035147 (2017).
- [37] N. Chikano, K. Yoshimi, J. Otsuki, and H. Shinaoka, ir-basis: Open-source database and software for intermediate-representation basis functions of imaginary-time green’s function, *Computer Physics Communications* **240**, 181 (2019).

- [38] P. Giannozzi, S. Baroni, N. Bonini, M. Calandra, R. Car, C. Cavazzoni, D. Ceresoli, G. L. Chiarotti, M. Cococcioni, I. Dabo, A. D. Corso, S. de Gironcoli, S. Fabris, G. Fratesi, R. Gebauer, U. Gerstmann, C. Gougoussis, A. Kokalj, M. Lazzeri, L. Martin-Samos, N. Marzari, F. Mauri, R. Mazzarello, S. Paolini, A. Pasquarello, L. Paulatto, C. Sbraccia, S. Scandolo, G. Sclauzero, A. P. Seitsonen, A. Smogunov, P. Umari, and R. M. Wentzcovitch, Quantum espresso: a modular and open-source software project for quantum simulations of materials, *Journal of Physics: Condensed Matter* **21**, 395502 (2009).
- [39] P. Giannozzi, O. Andreussi, T. Brumme, O. Bunau, M. B. Nardelli, M. Calandra, R. Car, C. Cavazzoni, D. Ceresoli, M. Cococcioni, N. Colonna, I. Carnimeo, A. D. Corso, S. de Gironcoli, P. Delugas, R. A. DiStasio, A. Ferretti, A. Floris, G. Fratesi, G. Fugallo, R. Gebauer, U. Gerstmann, F. Giustino, T. Gorni, J. Jia, M. Kawamura, H.-Y. Ko, A. Kokalj, E. Küçükbenli, M. Lazzeri, M. Marsili, N. Marzari, F. Mauri, N. L. Nguyen, H.-V. Nguyen, A. O. de-la Roza, L. Paulatto, S. Poncé, D. Rocca, R. Sabatini, B. Santra, M. Schlipf, A. P. Seitsonen, A. Smogunov, I. Timrov, T. Thonhauser, P. Umari, N. Vast, X. Wu, and S. Baroni, Advanced capabilities for materials modelling with quantum espresso, *Journal of Physics: Condensed Matter* **29**, 465901 (2017).
- [40] A. Dal Corso, Pseudopotentials periodic table: From h to pu, *Computational Materials Science* **95**, 337 (2014).
- [41] P. E. Blöchl, Projector augmented-wave method, *Phys. Rev. B* **50**, 17953 (1994).
- [42] G. Kresse and D. Joubert, From ultrasoft pseudopotentials to the projector augmented-wave method, *Phys. Rev. B* **59**, 1758 (1999).
- [43] J. P. Perdew, K. Burke, and M. Ernzerhof, Generalized gradient approximation made simple, *Phys. Rev. Lett.* **77**, 3865 (1996).
- [44] N. Marzari and D. Vanderbilt, Maximally localized generalized wannier functions for composite energy bands, *Phys. Rev. B* **56**, 12847 (1997).
- [45] I. Souza, N. Marzari, and D. Vanderbilt, Maximally localized wannier functions for entangled energy bands, *Phys. Rev. B* **65**, 035109 (2001).
- [46] A. A. Mostofi, J. R. Yates, Y.-S. Lee, I. Souza, D. Vanderbilt, and N. Marzari, wannier90: A tool for obtaining maximally-localised wannier functions, *Computer Physics Communications* **178**, 685 (2008).
- [47] G. Pizzi, V. Vitale, R. Arita, S. Blügel, F. Freimuth, G. Géranton, M. Gibertini, D. Gresch, C. Johnson, T. Koretsune, J. Ibañez-Azpiroz, H. Lee, J.-M. Lihm, D. Marchand, A. Marrazzo, Y. Mokrousov, J. I. Mustafa, Y. Nohara, Y. Nomura, L. Paulatto, S. Poncé, T. Ponweiser, J. Qiao, F. Thöle, S. S. Tsirkin, M. Wierzbowska, N. Marzari, D. Vanderbilt, I. Souza, A. A. Mostofi, and J. R. Yates, Wannier90 as a community code: new features and applications, *Journal of Physics: Condensed Matter* **32**, 165902 (2020).
- [48] K. Tanaka, Y. Yokoyama, and C. Hotta, Origin of biquadratic exchange interactions in a mott insulator as a driving force of spin nematic order, *Journal of the Physical Society of Japan* **87**, 023702 (2018), <https://doi.org/10.7566/JPSJ.87.023702>.
- [49] E. H. Lieb, The classical limit of quantum spin systems, in *Statistical Mechanics: Selecta of Elliott H. Lieb*, edited by B. Nachtergaele, J. P. Solovej, and J. Yngvason (Springer Berlin Heidelberg, Berlin, Heidelberg, 2004) pp. 433–446.
- [50] F. Körmann, A. Dick, T. Hickel, and J. Neugebauer, Rescaled monte carlo approach for magnetic systems: Ab initio thermodynamics of bcc iron, *Phys. Rev. B* **81**, 134425 (2010).
- [51] B. L. Gyorffy, Coherent-Potential approximation for a Nonoverlapping-Muffin-Tin-Potential model of random substitutional alloys, *Phys. Rev. B Condens. Matter* **5**, 2382 (1972).
- [52] A. Jacobsson, G. Johansson, O. I. Gorbatov, M. Ležaić, B. Sanyal, S. Blügel, and C. Etz, Efficient parameterisation of non-collinear energy landscapes in itinerant magnets, *Scientific Reports* **12**, 18987 (2022).
- [53] R. Singer, F. Dietermann, and M. Fähnle, Spin interactions in bcc and fcc fe beyond the heisenberg model, *Phys. Rev. Lett.* **107**, 017204 (2011).
- [54] A. J. Freeman, O. N. Mryasov, D. S. Wang, and R. Wu, Density functional theory of the electronic and magnetic properties of interfaces and multilayers, *Mater. Sci. Eng. B* **31**, 225 (1995).
- [55] D. Spišák and J. Hafner, Theory of bilinear and biquadratic exchange interactions in iron: Bulk and surface, *J. Magn. Magn. Mater.* **168**, 257 (1997).
- [56] X. He, N. Helbig, M. J. Verstraete, and E. Bousquet, Tb2j: A python package for computing magnetic interaction parameters, *Computer Physics Communications* **264**, 107938 (2021).
- [57] M. dos Santos Dias, S. Brinker, A. Lászlóffy, B. Nyári, S. Blügel, L. Szunyogh, and S. Lounis, Reply to “comment on ‘proper and improper chiral magnetic interactions’”, *Phys. Rev. B* **105**, 026402 (2022).
- [58] M. A. Ruderman and C. Kittel, Indirect exchange coupling of nuclear magnetic moments by conduction electrons, *Phys. Rev.* **96**, 99 (1954).
- [59] T. Kasuya, A theory of metallic ferro- and antiferromagnetism on zener’s model, *Progr. Theoret. Phys.* **16**, 45 (1956).
- [60] K. Yosida, Magnetic properties of Cu-Mn alloys, *Phys. Rev.* **106**, 893 (1957).